JOURNAL OF MATERIALS SCIENCE 31 (1996) 6485–6493

Machining refractory ceramics with abrasive water jets

A. W. MOMBER*
WOMA Apparatebau GmbH, 47208, Duisburg, Germany
I. EUSCH
Montanuniversität Leoben, 8700 Leoben, Austria
R. KOVACEVIC
University of Kentucky, Center for Robotics and Manufacturing Systems, Lexington, KY, 40506, USA

The material removal process of refractory ceramics cut by abrasive water jets was investigated. In particular, bauxite, sintered magnesia, and magnesia chromite, were cut in a wide range of pump pressures up to 350 MPa. The process parameters, such as pump pressure, traverse rate, abrasive flow rate, and abrasive type, were changed during the experiments in order to find an optimum parameter combination. For all experiments, the depth of cut, cut geometry, the surface structure of the generated cuts, and the material removal rates were measured and analysed. Based on these measurements the specific energies were estimated. Using scanning electron microscopy, it was found that the material removal mechanism changed with the depth of cut. In the upper region, the main material removal mechanism was the simultaneous cutting of matrix and inclusion grains (transgranular). In the lower range of the cut, the removal process was characterized by the removal of the binding matrix followed by washing of the inclusion grains (intergranular).

1. Introduction

The development of high-quality refractory materials by the ceramic industry brought to light latent problems with the machinability of the bricks being manufactured. To produce bricks of complex shape, advanced pressing methods, such as hot isostatic pressing, have been introduced. Unfortunately, this has led to high production costs and the produced refractory bricks have become very expensive.

Abrasive water jet (AWJ) machining could be one possible solution for manufacturing high-quality refractory bricks of special shapes and formats. Despite these needs, the number of serious investigations on the machinability of ceramics by AWJs is comparatively low. An early attempt to use this tool for the machining of ceramic materials was made by Kim *et al.* [1] who investigated ceramic stock removal using AWJ. They conducted piercing and cutting experiments on alumina ceramics and discussed the influence of several process parameters on the piercing process. They demonstrated that the AWJ could effectively be used to machine even high-strength ceramics. Neusen *et al.* [2] carried out cutting experiments on aluminium–silicon carbide and observed smearing of aluminium on the cut surface as well as embedding of fractured abrasive particles. They identified wear by individual abrasive particles as one of the micromechanisms of material removal. Later, Freist *et al.* [3] reported the application of AWJs for three-dimensional machining (milling) of alumina ceramics. This work included the development of a kerf geometry model as well as a limited parameter study. Hamatani and Ramulu [4] used AWJ for piercing of compound ceramics. They found random damage generated by the AWJ on the top surface of the pierced holes as well as non-linear hole tapers. They also detected a notable increase in the target temperature and concluded that AWJ machining of ceramics may not be totally free of thermal effects. Zeng and Kim [5] conducted SEM observations to evaluate the behaviour of sintered aluminium oxide ceramics subjected to AWJs under different jet impingement angles. They observed intergranular cracking and plastic flow as the two major material removal mechanisms. The intergranular fracture dominates the material removal mode in the normal impingement, and has equal significance to the plastic flow for the small angle impact. In an advanced investigation [6], these authors developed a material removal model as well as a kerf cutting model for brittle materials processed by AWJs. To verify their

*Feodor Lynen Scholar of the Alexander-von-Humboldt Foundation, Bonn, Germany, at the University of Kentucky, Lexington, KY, USA.

0022–2461

model, they carried out cutting experiments under different process conditions, such as different pump pressures, traverse rates, abrasive flow rates, and AWJ nozzle diameter. Nevertheless, Momber *et al.* [7] found that intergranular fracture dominates the removal process only in materials that are characterized by a low-strength matrix and fine inclusion grains. For materials with comparatively high matrix strength and coarse inclusions, cracking occurs through the matrix as well as through the inclusion grains, and the failure is dominated by transgranular fracture. Ramulu *et al.* [8] machined composite ceramics by AWJ at shallow impacting angles and observed erosion by microcutting in the matrix, whereas the inclusions were removed by the shovelling action of the on-coming jet.

In contrast to the kinetic process models, Kahlman *et al.* [9] who observed the formation of high local temperatures (about 1280 °C) on the surfaces of ceramics during the AWJ cutting process, introduced the failure of ceramic materials by thermal spalling. They assumed that the cooling by the water flow creates local stress fields. Based on scanning electron micrographs and wear volume measurements, these references defined the thermal shock resistance, R', as the main resistance parameter against AWJ machining action and defined a machining limit for ceramics at $R' = 15\ \mathrm{W\,mm^{-1}}$. Above this value, the material removal rapidly decreases.

Hochyeng and Chang [10] reported volume removal studies on aluminium oxide and silicon nitride ceramics. In their study, they investigated the influence of several process parameters, such as pump pressure and abrasive flow rate, on material removal rate and surface quality. Nevertheless, no attempt was made to discuss the presented experimental results in terms of basic material removal mechanisms.

2. Experimental procedure

Three different types of commercial refractory ceramics were used in this study. The mechanical properties of the materials are listed in Table I. Sintered magnesia bricks are used as lining material for steel and cement furnaces. Magnesia consist mainly of periclase (95%). It has a high melting point and a high Young's modulus and behaves in a very brittle manner under load. Magnesia chromite is used for the lining of steel and cement furnaces, and for non-ferrous metal kilns where high spalling resistance and high-temperature resistance are needed. The chromite phase reduces the Young's modulus and induces some capability of plastic deformation. Bauxite bricks are commonly used in the steel industry. The material mainly contains corundum (50%–70%) and mullite (25%–35%). Bauxite has an average Young's modulus and a relatively high compressive strength. Generally, the temperature resistance is low.

The abrasive water jet cutting unit used in this study consists of an intensifier pump to produce the high water pressure, an abrasive water jet cutting head, an abrasive storage and metering system, a catcher, and an $x - y - z$ positioning table. The abrasive water jet cutting head, which hosts the chamber for the mixing between the high-pressure water and the entrained abrasive particles, as well as the focus for the acceleration of the abrasive particles, is shown in Fig. 1. The cutting conditions are listed in Table II. After cutting, the depth of cut, h, and the width of the cut, b, were estimated as the average of five measurements on every cut. The material removal rate, $\dot{V}_M$, was calculated from

$$\dot{V}_{\mathrm{M}} = hbv \tag{1}$$

where v is the traverse rate. The specific energy of the material removal process, E_{SP}, was calculated using

$$E_{\mathrm{SP}} = \frac{E_{\mathrm{A}}}{hbL} \tag{2}$$

where E_{A} is the kinetic energy of the AWJ, and L is the length of the cut. For the surface measurements, a mechanical roughness measurement unit was used with different cut-offs.

TABLE I Mechanical properties of the investigated refractory ceramics

Material	Density ($\mathrm{g\,cm^{-3}}$)	Porosity (%)	Cold compressive strength (MPa)	Cold bending tensile strength (MPa)	Young's modulus (MPa)
Bauxite	2.89	15	126	19	59000
Sintered magnesia	3.00	15 ± 2	40	14	85000
Magnesia chromite	3.26	15 ± 2	30	3.5	13000

TABLE II Abrasive water jet cutting conditions

Pump pressure (MPa)	Traverse rate ($\mathrm{mm\,s^{-1}}$)	Abrasive flow rate ($\mathrm{g\,s^{-1}}$)	Abrasive type	Focus diameter (mm)	Focus length (mm)	Orifice diameter (mm)
100–350	0.5–8.0	4.54–14.82	Garnet 36 Corundum 100	1.27	88.9	0.389

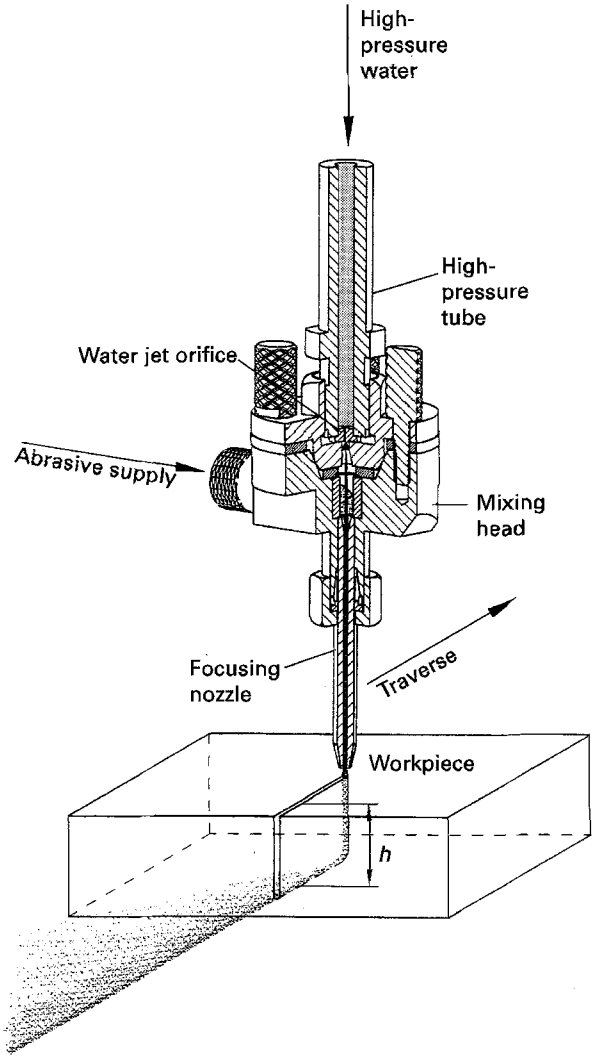

Figure 1 Structure and performance of the used abrasive water jet cutting head.

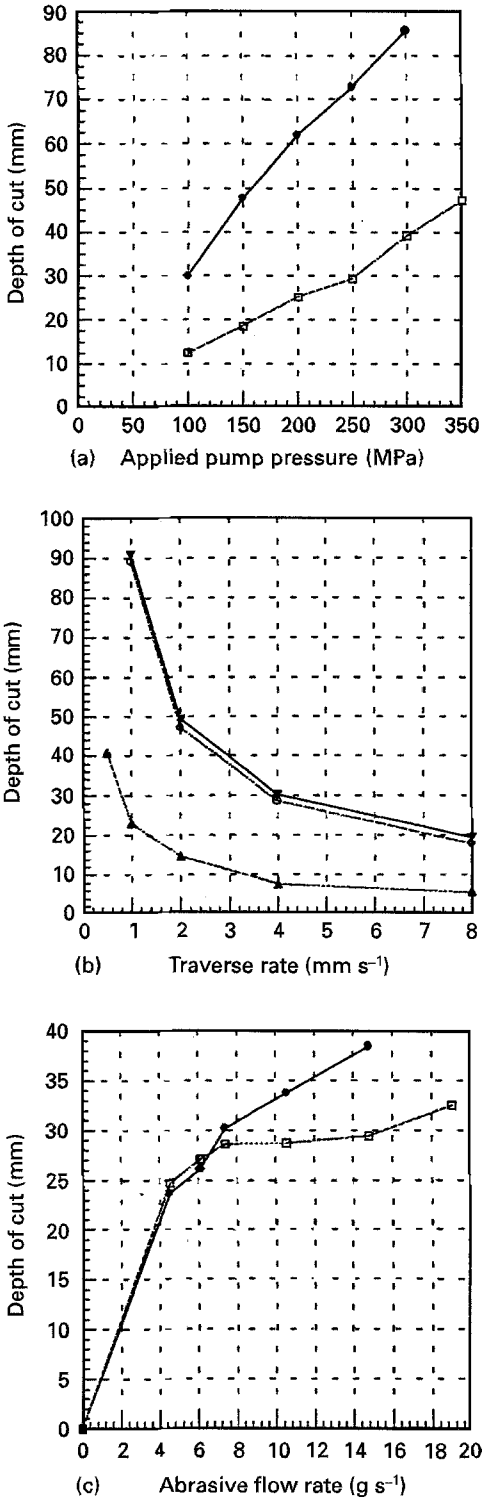

Figure 2 Influence of (a) pump pressure, (b) traverse rate, and (c) abrasive flow rate, on the depth of cut in refractory ceramic samples: (a) abrasive (□) garnet 36, (●) corundum 100; (b) material (▲) bauxite, (○) magnesia, (▼) magnesia chromite; (c) material (□) magnesia, (●) magnesia chromite.

3. Results and discussion

3.1. Aspects of process parameter optimization

In order to optimize the cutting process, the most important process parameters from the practical point of view, such as pump pressure, p, traverse rate, v, abrasive flow rate $\dot{m}_P$, and abrasive type, were varied.

Fig. 2a shows the influences of the applied pump pressure and of the abrasive type on the depth of cut. The generally linear trend, as shown in this figure, was observed under all cutting conditions and for all materials. The mathematical expression is

$$h(p) = C_1 \cdot (p - p_{thr}) \quad (3)$$

The same qualitative trend is shown in Fig. 3a for the relation between the applied pump pressure and the volume removal rate, confirming results given elsewhere [10]. In Equation 3, the parameter p_{thr} is the threshold pressure which describes a critical abrasive velocity which must be overcome to introduce the damage process under the given conditions. There is some evidence from solid particle erosion investigations on ceramics [11], as well as from abrasive water jet cutting experiments in concretes [12], that this parameter may be related to the P-wave velocity in the material. It is interesting to note that the threshold pressure of the sintered bauxite is not very sensitive to the abrasive type. For both abrasive materials the threshold pressure is about $p_{thr} = 25$ MPa. In contrast, the established cutting process ($p > p_{thr}$) is very strongly influenced by the abrasive type. Using corundum for cutting, the depth of cut can be doubled

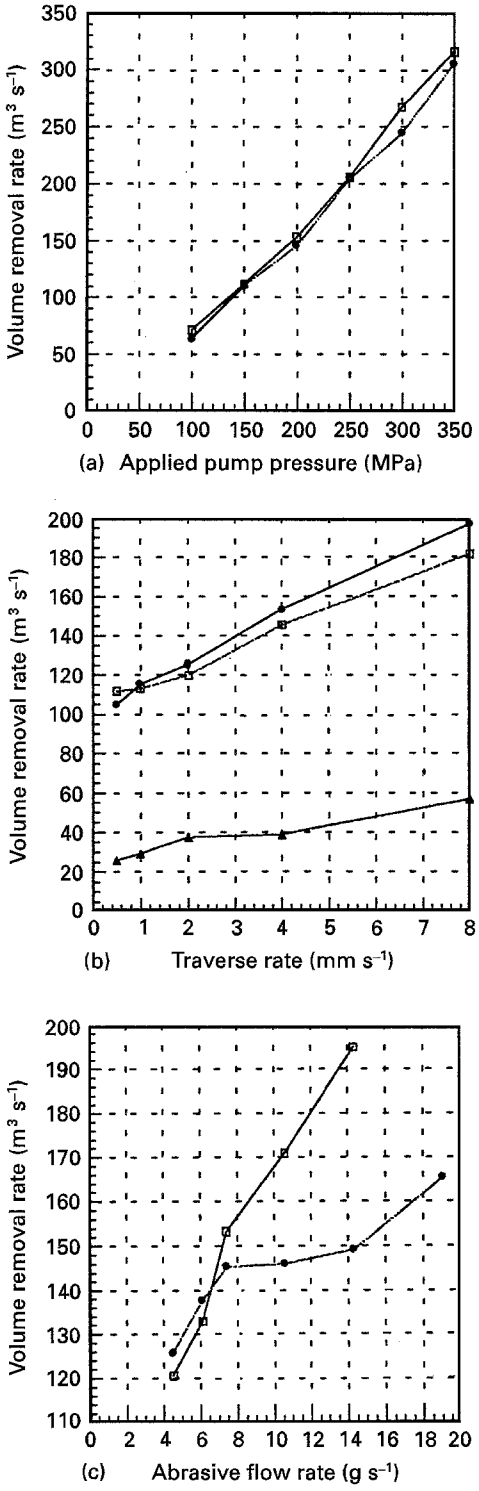

Figure 3 Influence of (a) pump pressure, (b) traverse rate, and (c) abrasive flow rate on the material removal rate in refractory ceramics: (a) (●) magnesia, (□) magnesia chromite; (b) (□) magnesia, (●) magnesia chromite, (▲) bauxite; (c) (●) magnesia, (□) magnesia chromite.

over almost the entire pressure range. Therefore, the constant C_1 in Equation 3 may be very sensitive to the abrasive type. This may be due to the higher hardness of the corundum abrasive particles. Also, the influence of the abrasive type increases with an increase in the pump pressure. In Fig. 4a the specific energy is plotted versus the applied pump pressure. The high values for bauxite are due to the lower traverse rate used for this material. For this material the specific energy shows a strong relation to the pump pressure for low and medium pressures. In contrast, the specific energy values of the sintered magnesia samples are not significantly influenced by the applied pump pressure. They show only a weak linear progress.

The influence of the traverse rate on the depth of cut is shown in Fig. 2b. These relations can reasonably be approximated by a parabolic equation as

$$h(v) = \frac{C_2}{v^{C_3}} \tag{4}$$

The materials are sensitive to changes in the traverse rate, especially in the range of low traverse rates (up to $v = 4\ \mathrm{mm\,s^{-1}}$). For traverse rates beyond this value, there is no significant change in the depth of cut. A different trend is shown in Fig. 3b for the relation between traverse rate and material volume removal rate. In this case, the trend is almost linearly increasing. Every increase in the traverse rate leads to a corresponding increase in the volume removed per unit time. This observation is important for milling and turning of the refractory ceramic materials with abrasive water jets. These results suggest that despite the drop in the depth of cut for high traverse rates (Fig. 3a) the material removal process is more efficient at high traverse rates, probably because of the reduced friction and damping effects in the shallower cuts. As a result of these processes, the specific energy drops approximately linearly as the traverse rate increases (Fig. 4b). This tendency is very clear for the bauxite sample which also requires comparatively high specific material removal energies.

Fig. 2c shows the relation between the abrasive flow rate and the depth of cut. There is a linear trend with a constant progress for both materials for low abrasive flow rates. Later, at about $\dot{m}_p = 5\ \mathrm{g\,s^{-1}}$, the progress drops (for the magnesia chromite) or even stops (for the sintered magnesia), respectively. A mathematical expression to describe these relations may be

$$h(\dot{m}_P) = h_0(1 - e^{-C_4 \cdot \dot{m}_P}) \tag{5}$$

where h_0 is a maximum depth of cut which can be achieved under the given cutting conditions. It is very interesting that the ceramic materials behave identically for low abrasive flow rates. But beyond an abrasive flow rate of about $\dot{m}_P = 8\ \mathrm{g\,s^{-1}}$ the functions for the materials are very different. In this range, the magnesia chromite shows a significant increase in the depth of cut with rising abrasive flow rate, whereas the depth of cut in sintered magnesia remains approximately constant. A further increase in the abrasive flow rate does not lead to any improvement of the cutting process in the sintered magnesia. Therefore, the parameter h_0 in Equation 5 is much higher for the magnesia chromite. The reason for the different behaviour may be the fact that the magnesia chromite is able to react with some plastic deformations to the abrasive particle impact. Therefore, a multiple particle impact may improve the material removal process and, as the number of impacting particles increases, the material removal will also continue to increase. In contrast, the very brittle behaving sintered magnesia is much more

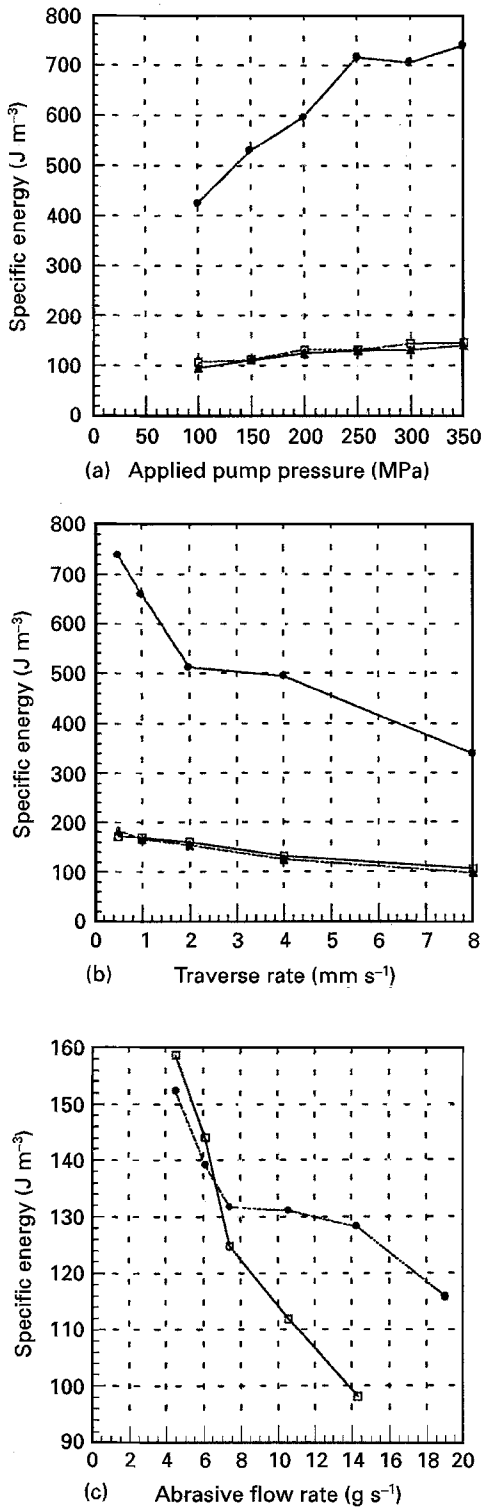

Figure 4 Influence of (a) pump pressure, (b) traverse rate, and (c) abrasive flow rate, on the specific removal energy in refractory ceramics: (a) (□) magnesia, (▲) magnesia chromite, (●) bauxite; (b) (▲) magnesia chromite, (□) magnesia, (●) bauxite; (c) (●) magnesia, (□) magnesia chromite.

sensitive to the impact energy of the single particles than to the particle impact frequency. Because the average abrasive impact velocity decreases with an increase in the abrasive mass flow rate [13], a further increase in the abrasive flow rate does not bring any benefit for the material removal process and the depth of cut cannot be increased further. These observations also show that the equal depths of cut for both these materials presented in Fig. 2b are valid only for comparatively small abrasive flow rates.

Fig. 3c exhibits the relation between the abrasive flow rate and the material volume removal rate. For the magnesia chromite, the trend is linear with a constant progress over the investigated abrasive flow rate range. In contrast, the curve for the sintered magnesia shows a significant drop in the progress at abrasive flow rates larger than $\dot{m}_P = 8\,g\,s^{-1}$. These observations are in agreement with the conditions shown in Fig. 1c and can be explained by using the same arguments as below.

The specific energy drops with an increase in the abrasive flow rate as illustrated in Fig. 4c. The drop is linear with a very sharp progress for the magnesia chromite over the entire parameter range, as well as for the sintered magnesia in the range of small abrasive flow rates.

3.2. Aspects of cut quality

Fig. 5a shows the relation between the applied pump pressure and the width of the cut in magnesia chromite. The measured values are comparable to cut width measurement results given elsewhere [10]. There is no general tendency detectable in Fig. 5a, but it can be seen that most of the cuts are tapered. Usually the top width is smaller than the width on the bottom of the cut. Exceptions are the cuts generated with pressures at $p = 150$ and 250 MPa where the top width and the bottom width of the cuts are equal.

In Fig. 5b the cut widths are plotted against the traverse rate. There is a general trend visible that the cut widths on both locations, especially on the top, can be reduced by increasing the traverse rate. The same trend was observed previously [10] for alumina ceramics. Also, the taper can significantly be reduced with higher traverse rates. It is interesting to note a transition point at a traverse rate between $v = 3$ and $4\,mm\,s^{-1}$. At this point, the direction of the taper changes, or in other words, the width on the top of the cut exceeds that on the bottom of the cut. It was also observed that the average roughness of the cut surface decreases slightly with increasing traverse rate.

The influence of the abrasive flow rate on the cut geometry is shown in Fig. 5c. The width of the cut on the top as well as on the bottom increases almost linearly with increasing abrasive flow rate. Here, also, a transition point can be noticed at an abrasive flow rate of $\dot{m}_P = 12\,g\,s^{-1}$.

Fig. 6 shows the relation between the abrasive flow rate and the average surface roughness estimated on bauxite samples. The roughness values of about $R_a = 20\,\mu m$ are comparatively high compared to those measured elsewhere [10] for alumina ceramics ($R_a \cong 1.5\,\mu m$). The reason may be the different locations of the roughness measurements in both studies. Hochyeng and Chang [10] used thin ceramic plates (thickness between 5 mm and 10 mm) and cut them through, which usually yields low roughness values. Also, differences in the structure of the investigated materials may play a role. It can be seen from Fig. 6 that the average roughness decreases with increasing

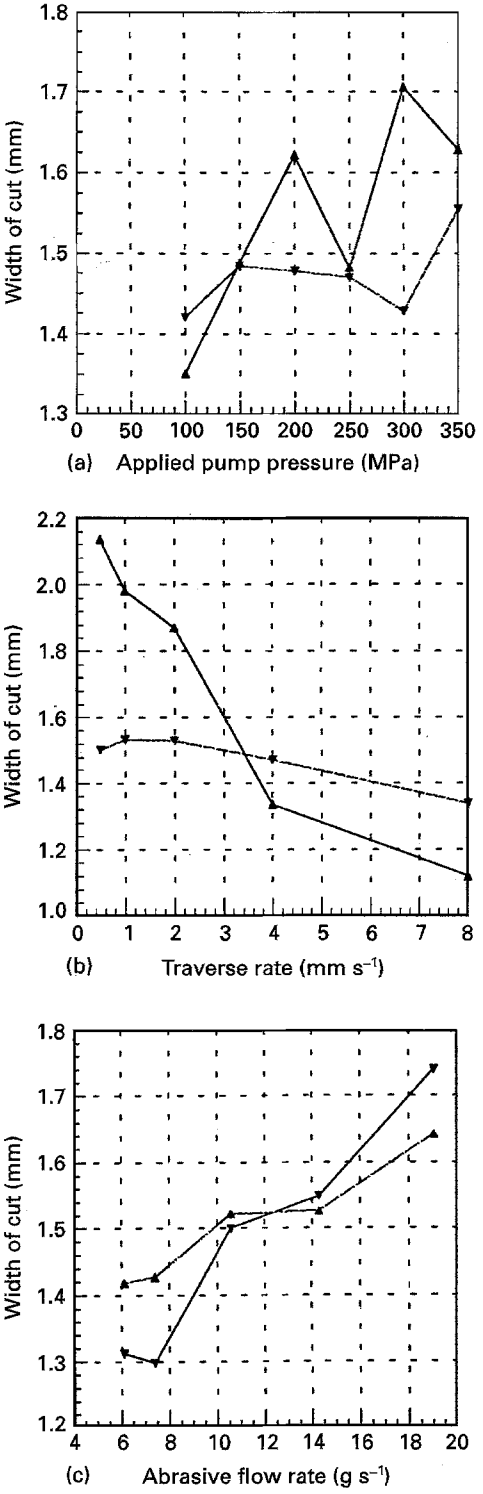

Figure 5 Influence of (a) pump pressure, (b) traverse rate, and (c) abrasive flow rate on the cut geometry in refractory ceramics: (a) magnesia chromite, (▼) top, (▲) bottom; (b) magnesia, (▼) top, (▼) bottom; (c) bauxite, (▲) top, (▼) bottom.

abrasive flow rate. Fig. 7 shows that the average roughness of the cut surface is significantly higher for AWJ cutting compared to diamond saw cutting.

3.3. Material removal process observations

To understand the material removal processes involved in the machining of the ceramic materials, SEM studies have been carried out on all materials under different cutting conditions and at different

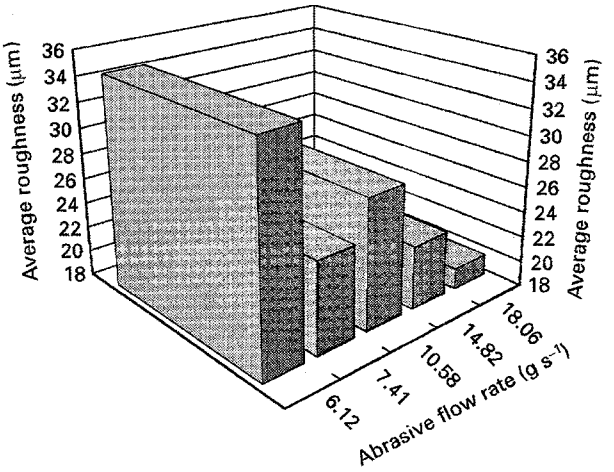

Figure 6 Relation between abrasive flow rate and roughness (material: bauxite).

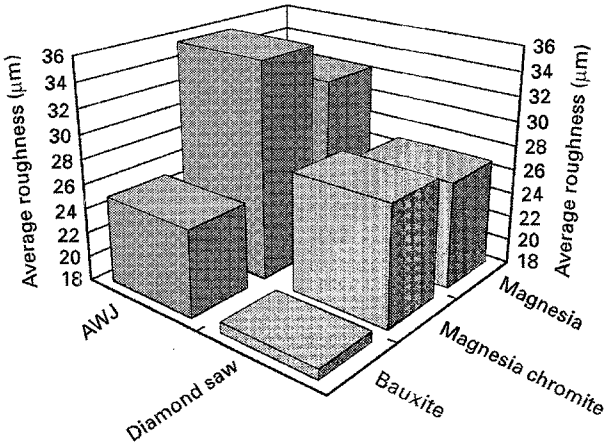

Figure 7 Surface roughness of refractory ceramics cut by a diamond saw and an abrasive water jet.

locations. Typically, the abrasive water jet entry zone (top of the cut) and the abrasive water jet exit zone (bottom of the cut) are examined by the SEM technique.

Fig. 8a shows a scanning electron micrograph of the entry zone of a cut of a magnesia sample cut by AWJ. In the right top region, a very smooth cut surface can be noticed, including open pores as observed during the brittle fracture of the material in the tensile test. The left side of the photograph shows periclase fragments. Obviously, the periclase grains are fractured due to the AWJ action. In this range, open pores with sharp edges can be seen, too. The material removal process can be characterized by transgranular fracture through matrix and inclusions. The situation is very different in Fig. 8b, which shows the exit zone of the same cut. Here, the periclase grains are completely intact (left region) or partially cracked (central region) but the matrix between them is removed. The figure shows that penetrating cracks are stopped by the hard periclase inclusions. No open pores were found. These observations indicate an intergranular material removal mode in the lower region of the cut. The small particles attached on the periclase surface are brucites formed due to the hydration of the magnesia oxide in the periclase grains.

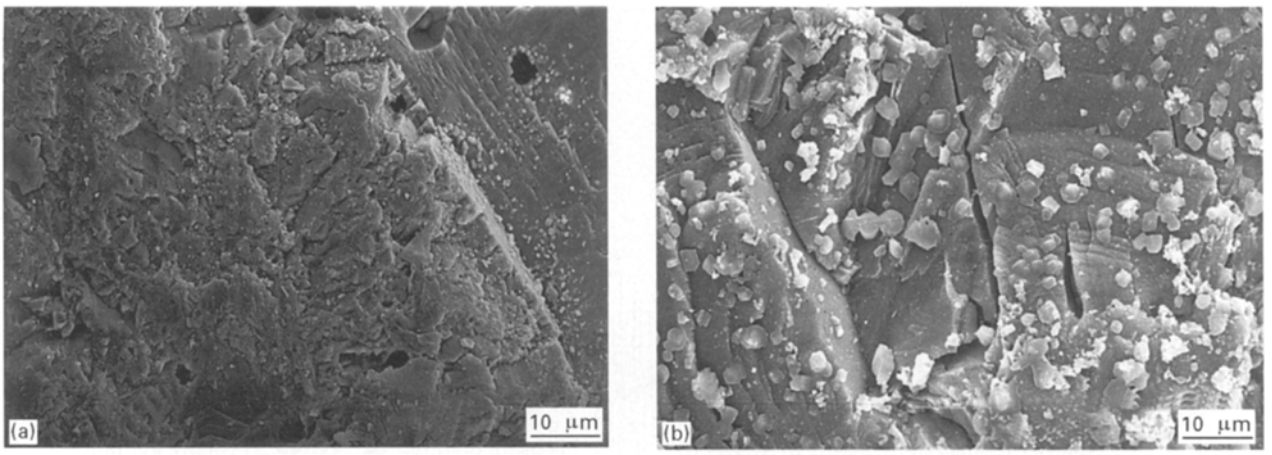

Figure 8 Scanning electron micrographs of AWJ (a) entry and (b) exit zones in magnesia. (a) Smooth pores, fractured periclase grain, small fracture areas; (b) crack arresting in periclase grain, bauxite formation on the grain surface.

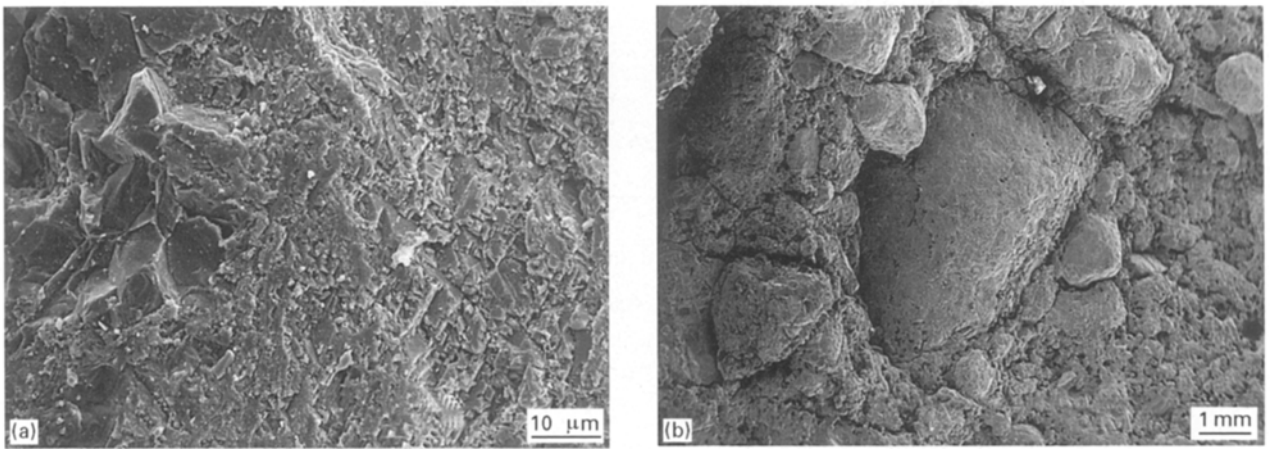

Figure 9 Scanning electron micrographs of AWJ (a) entry and (b) exit zones in magnesia chromite. (a) Periclase and chromite grains are fractured; (b) periclase grain (centre) and chromite grains are destroyed.

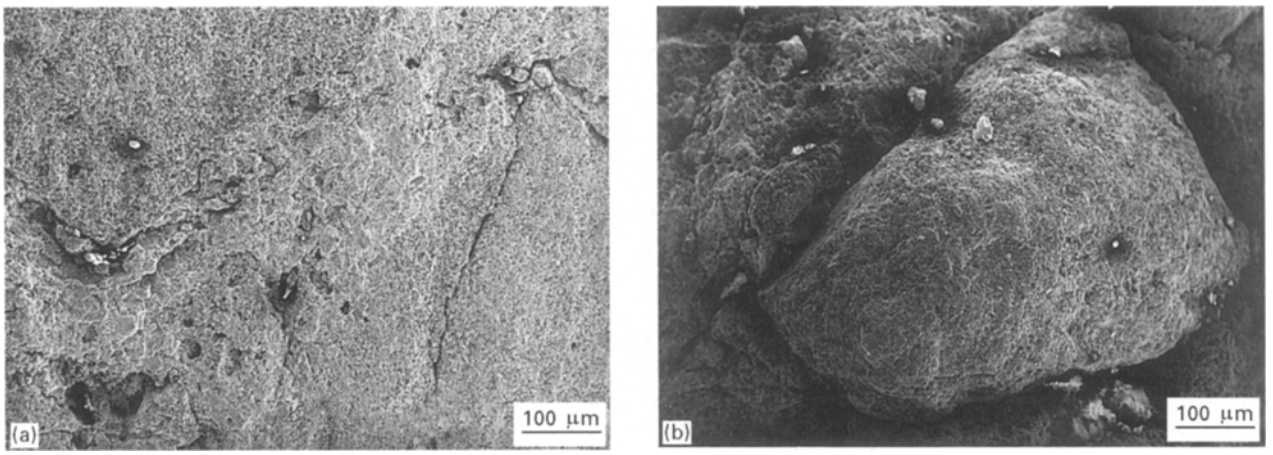

Figure 10 Scanning electron micrographs of AWJ (a) entry and (b) exit zones in bauxite. (a) Clear cut, grain-boundary remains intact; (b) grain in washed out, surrounding matrix is removed.

The failure mechanisms in the magnesia chromite are illustrated in Fig. 9. In the upper zone of the cut (Fig. 9a), the periclase grains (left region) are broken; the fracture areas are comparatively large. The right region in Fig. 9a shows fine-grained fragments of a broken chromite grain. The situation in the exit zone of the cut is shown in Fig. 9b using a smaller magnification. In the central region of the photograph a large, completely undestroyed periclase grain can be seen. Also, on the upper left edge of this grain, a group of unfractured chromite grains is located.

Similar features are observed in the bauxite samples. Fig. 10a, which is a scanning electron micrograph from the upper part of the cut shows, for example, that the grain boundary at the corundum grains remains intact after the abrasive water jet

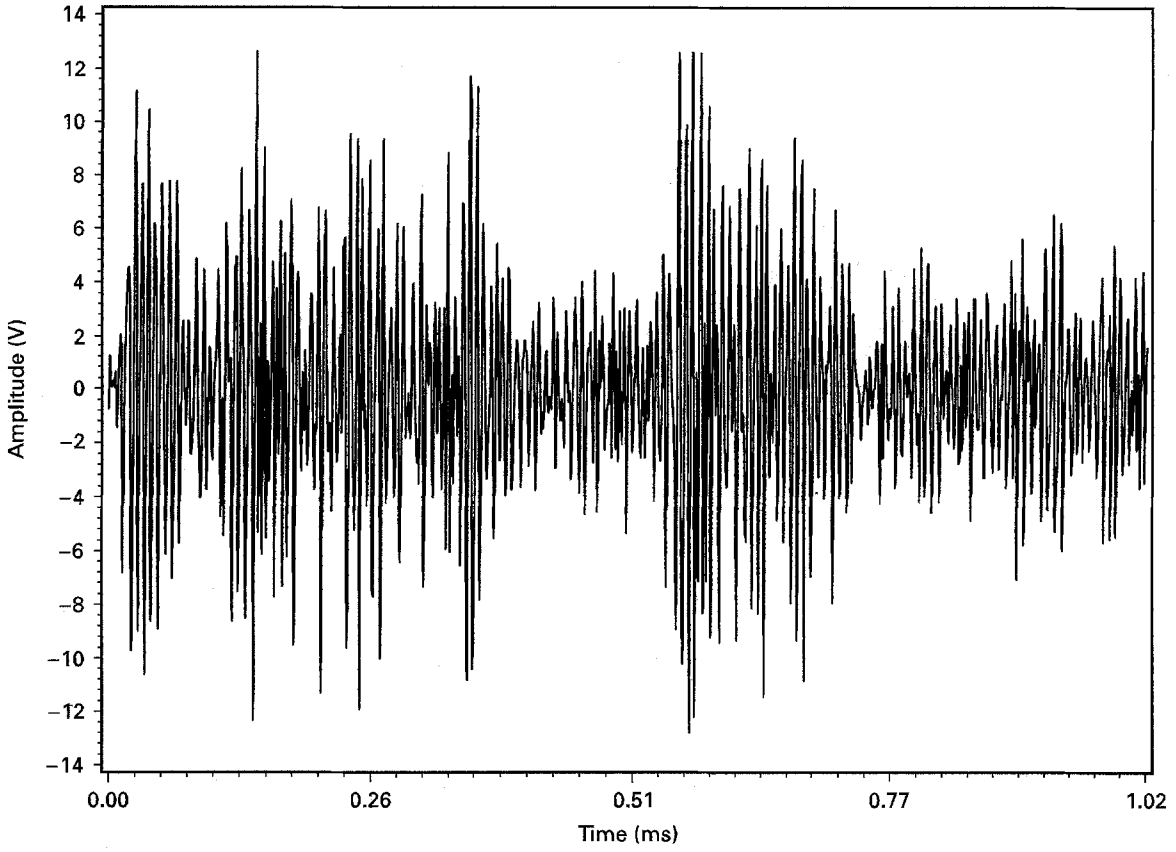

Figure 11 Time domain AE signal, Bauxite. (—) $p = 200$ MPa, V = 1.0 mm s^{-1}, $m = 7.41$ g s^{-1}.

attack. The failure runs completely through both the grains and the matrix. For the bottom region of the generated cut, the situation is illustrated in Fig. 10b. Here, a removed corundum grain is shown, as well as evidence that the surrounding matrix material is removed by the abrasive water jet. The corundum grain is still rounded, which suggests that it is probably pulled out by the action of the flowing water in the kerf after the matrix was removed.

A systematic observation of the entire cutting fronts (from the entry to the exit) did not give any indication of an abrupt change in the material removal mechanisms for the investigated materials. The transition from transgranular fracture on top of the cut to the intergranular removal process on the bottom of the cut is steady. This result supports the idea of a continuous energy loss of the abrasive water jet in the cut as recently supposed by Momber and Kovacevic [13,14] and Raju and Ramulu [15]. In the beginning of the cutting process, the single abrasive grains have sufficient kinetic energy to contribute to the cutting process. In the upper cut region, the energy of the abrasive water jet is high enough to cut the harder periclase grains (periclase Vickers hardness, for example, was measured to be about 700 kg mm^{-2}). Due to friction, damping and generation of wear particles, the AWJ will lose part of its kinetic energy during the cutting process. On the lower part of the cut the abrasive water jet, which has a reduced kinetic energy, can no longer destroy the inclusions, but can only remove the weaker matrix between single inclusion grains.

This unsteady material removal process is reflected by the structure of a time-domain acoustic emission signal which was acquired during the abrasive water jet cutting of a bauxite specimen. As shown in Fig. 11, the acoustic signal shows several burst emissions. This type of emission usually corresponds to events of sudden energy release, such as spalling fracture. Probably, the burst emissions are expressions of the fracture of the inclusion grains. This process may generate high energy stress waves which are detected by the acoustic emission technique.

4. Conclusions

1. Abrasive water jets can generally be used to machine high-quality refractory ceramics (bauxite, sintered magnesia, magnesia chromite).

2. Material volume removal rates between $\dot{V}_M = 200$ mm^3 s^{-1} and $\dot{V}_M = 300$ mm^3 s^{-1} are achievable by using optimum process parameter combinations. High pump pressures, high traverse rates, and high abrasive flow rates are beneficial to the cutting process. The use of corundum as abrasive material can double the cutting efficiency compared to garnet for the materials investigated in this study.

3. The specific material removal energy can be optimized. The lowest value obtained in this study was $E_{SP} = 100$ J mm^{-3}. Medium pump pressures, high traverse rate, and high abrasive flow rate are the most beneficial.

4. The optimum process parameter constellation, especially the evaluation of the abrasive flow rate, is strongly related to the behaviour of the machined material.

5. The cuts generated by abrasive water jets are generally tapered.

6. The roughness of the abrasive water-jet generated surfaces is high compared to surfaces created by diamond saw cutting. The roughness depends on the applied process parameters as well as on the processed material. The roughness is low for bauxite and high for magnesia chromite.

7. The material removal process is a mixture between transgranular fracture and intergranular fracture. In the upper cutting zone, transgranular fracture dominates, whereas the bottom zone is characterized by intergranular fracture. These observations are explained by using the model for a continual loss in kinetic energy of the abrasive water jet during the cutting process.

Acknowledgements

The authors thank the Alexander-von-Humboldt Foundation, Bonn, Germany, and the Center for Robotics and Manufacturing Systems, University of Kentucky, Lexington, KY, for financial support. Veitsch Radex AG, Austria, is thanked for delivering the refractory ceramic specimens.

References

1. T. J. KIM, G. SYLVIA and L. POSNER, *ASME PED* **17** (1985) 19.
2. K. F. NEUSEN, P. K. ROHATGI and D. ALBERTS, in "Proceedings of the 4th US Water Jet Conference", edited by D. Dornfeld and M. Hood (ASME, New York, 1987) p. 175.
3. B. FREIST, H. HAFERKAMP, A. LAURINAT and H. LOUIS, in "Proceedings of the 5th American Water Jet Conference", edited by M. M. Mohan and G. A. Savanick (Water Jet Technology Association, St Louis, 1989) p. 191.
4. G. HAMATANI and M. RAMULU, *ASME J. Eng. Mater. Technol.* **112** (1990) 381.
5. J. ZENG and T. J. KIM, Int. J. Water Jet Technol. **1** (1991) 65.
6. *Idem*, in "Jet Cutting Technology", edited by A. Lichtarowicz, (Kluwer Academic, Dordrecht, 1992) p. 483.
7. A. MOMBER, R. S. MOHAN and R. KOVACEVIC, in proceedings of the 1st International Machining and Grinding Conference, edited by S. Malkin and W. Z. Zdeblick (Society of Manufacturing Engineers, Dearburn, 1995) p. 69.
8. M. RAMULU, S. P. RAJU, H. INOUE and J. ZENG, *Wear* **166** (1993) 55.
9. L. KAHLMAN, S. KARLSSON, R. CARLSSON and C. G. NILSSON, *Am. Ceram. Soc. Bull.* **72** (1993) 93.
10. H. HOCHYENG and K. R. CHANG, *J. Mater. Proces. Technol.* **40** (1994) 287.
11. G. A. EVANS, in "Fracture Mechanics of Ceramics", 1978, edited by R. C. Brandt, D. P. Hasselmann and F. F. Lange (Plenum Press, New York, 1978) p. 303.
12. A. MOMBER, R. KOVACEVIC and I. EUSCH, in "Rock Mechanics", edited by J. J. Daemen and R. A. Schultz (Balkema, Rotterdam, 1995) p. 355.
13. U. HIMMELREICH, PhD thesis, University of Hanover (1992).
14. A. MOMBER and R. KOVACEVIC, in "Manufacturing Science and Engineering", Vol. 1 (ASME, New York, 1994) p. 361.
15. A. MOMBER and R. KOVACEVIC, *Inst. Mech. Eng. J. Eng. Manuf.* **209** (1995) 491.
16. S. P. RAJU and M. RAMULU, *Manuf. Sci. Eng.* **1** (ASME, New York, 1994)p. 339.

Received 25 September 1995
and accepted 18 March 1996